Cell Reports
Methods

Article

GEM-IL: A highly responsive fluorescent lactate indicator

Graphical abstract

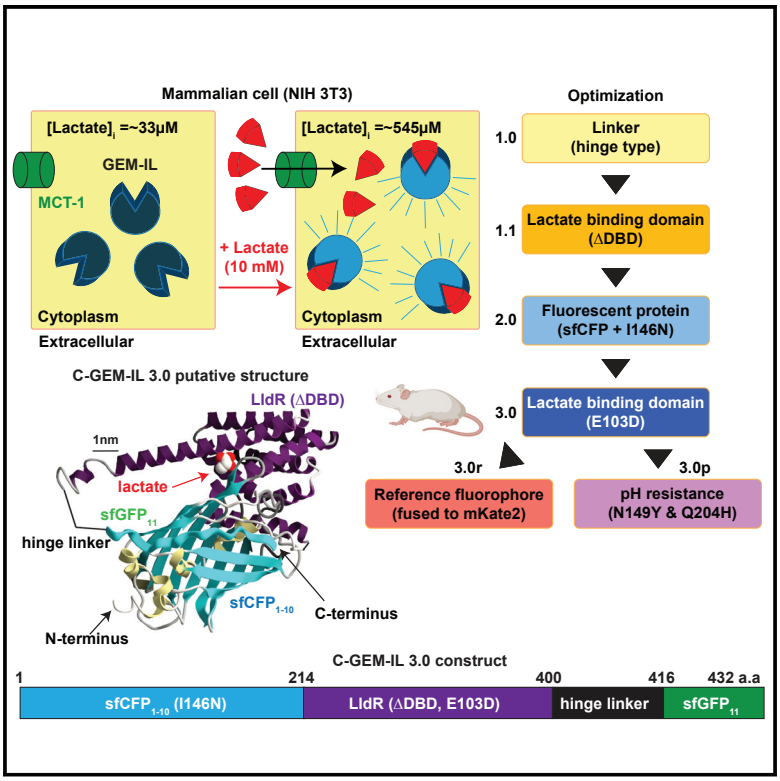

Highlights

- Development of a genetically encoded metabolic indicator for lactate (GEM-IL)
- Mutagenesis and fluorophore alteration improve responsivity and specificity to lactate
- *In vivo* model generation, validation, and application of GEM-IL
- GEM-IL shows improved sensitivity over currently available lactate indicators

Authors

Ramsey Bekdash, Jose R. Quejada, Shunnosuke Ueno, ..., Alexander I. Sobolevsky, Keisuke Goda, Masayuki Yazawa

Correspondence

my2387@columbia.edu

In brief

Bekdash et al. report the development of a genetically encoded metabolic indicator for probing lactate (GEM-IL) based on superfolder fluorescent proteins and mutagenesis. With improvements in the design, specificity, and sensitivity, the authors demonstrate GEM-IL's usefulness and functionality compared with previous lactate indicators, Laconic and Green Lindoblum.

Bekdash et al., 2021, Cell Reports Methods *1*, 100092
November 22, 2021
https://doi.org/10.1016/j.crmeth.2021.100092

CellPress

Cell Reports Methods

CellPress
OPEN ACCESS

Article

GEM-IL: A highly responsive fluorescent lactate indicator

Ramsey Bekdash,[1,2,3,12] Jose R. Quejada,[1,2,3,12] Shunnosuke Ueno,[1,2,4,12] Fuun Kawano,[1,2] Kumi Morikawa,[1,2] Alison D. Klein,[1,2] Kenji Matsumoto,[5] Tetz C. Lee,[5] Koki Nakanishi,[5] Amy Chalan,[1,2] Teresa M. Lee,[1,6] Rui Liu,[5] Shunichi Homma,[5] Chyuan-Sheng Lin,[7,8] Maria V. Yelshanskaya,[9] Alexander I. Sobolevsky,[9] Keisuke Goda,[4,10,11] and Masayuki Yazawa[1,2,3,13,*]

[1]Columbia Stem Cell Initiative, Columbia University, New York, NY 10032, USA
[2]Department of Rehabilitation and Regenerative Medicine, Vagelos College of Physicians and Surgeons, Columbia University, 650 West 168th Street, BB1108/BB1109D, New York, NY 10032, USA
[3]Department of Molecular Pharmacology and Therapeutics, Vagelos College of Physicians and Surgeons, Columbia University, New York, NY 10032, USA
[4]Department of Chemistry, University of Tokyo, Tokyo 113-0033, Japan
[5]Division of Cardiology, Department of Medicine, Vagelos College of Physicians and Surgeons, Columbia University, New York, NY 10032, USA
[6]Department of Pediatrics, Vagelos College of Physicians and Surgeons, Columbia University, New York, NY 10032, USA
[7]Department of Pathology and Cell Biology, Vagelos College of Physicians and Surgeons, Columbia University, New York, NY 10032, USA
[8]Transgenic Mouse Shared Resource, Herbert Irving Comprehensive Cancer Center, Columbia University, New York, NY 10032, USA
[9]Department of Biochemistry and Molecular Biophysics, Vagelos College of Physicians and Surgeons, Columbia University, New York, NY 10032, USA
[10]Department of Bioengineering, University of California, Los Angeles, CA 90095, USA
[11]Institute of Technological Sciences, Wuhan University, Hubei 430072, China
[12]These authors contributed equally
[13]Lead contact
*Correspondence: my2387@columbia.edu
https://doi.org/10.1016/j.crmeth.2021.100092

MOTIVATION The ability to detect and monitor changes in lactate at the cellular level is essential for understanding various physiological systems. Current methods have limited sensitivity and low intracellular expression, and there are no genetically encoded *in vivo* models available. To address these issues and monitor changes in lactate, we have developed, optimized, and characterized a genetically encoded metabolic indicator for lactate (GEM-IL). This tool is a reliable method for studying metabolic activity as demonstrated *in vitro* and *in situ*. In addition, we have developed an *in vivo* murine model for this indicator for further applications in metabolism study.

SUMMARY

Lactate metabolism has been shown to have increasingly important implications in cellular functions as well as in the development and pathophysiology of disease. The various roles as a signaling molecule and metabolite have led to interest in establishing a new method to detect lactate changes in live cells. Here we report our development of a genetically encoded metabolic indicator specifically for probing lactate (GEM-IL) based on superfolder fluorescent proteins and mutagenesis. With improvements in its design, specificity, and sensitivity, GEM-IL allows new applications compared with the previous lactate indicators, Laconic and Green Lindoblum. We demonstrate the functionality of GEM-IL to detect differences in lactate changes in human oncogenic neural progenitor cells and mouse primary ventricular myocytes. The development and application of GEM-IL show promise for enhancing our understanding of lactate dynamics and roles.

INTRODUCTION

Lactate, once viewed simply as a waste product, has garnered increasing importance as a metabolite and signaling molecule that is shuttled between cells and organs (Adeva-Andany et al., 2014; Philp et al., 2005). As proteins, fats, and polysaccharides are broken down and generated via catabolic and anabolic pathways, lactate plays a critical metabolic role. As a major source of

energy and signaling molecule, the importance of lactate in glycolysis, gluconeogenesis, and the citric acid cycle has been well documented (Baltazar et al., 2020; Goodwin et al., 2007; Takahashi and Yamada, 1996). Neurologically, it has been identified as a component of brain energy metabolism and may also act as an important signaling molecule that controls food intake in response to glucose levels (Boumezbeur et al., 2010; Cortes-Campos et al., 2013; Magistretti and Allaman, 2018). Neuronal energetics has focused on the metabolic relationships of glucose, pyruvate and lactate accumulation, and shuttling between astrocytes and neurons (Diaz-Garcia et al., 2017; Lerchundi et al., 2015; Machler et al., 2016; Vardjan et al., 2018). In arterial blood, lactate concentrations have been negatively correlated to patient survival following an ischemic event such as myocardial infarction, as well as septic shock (Hattori et al., 1985; Kawase et al., 2015; Lee and An, 2016). In oncology, cells prone to metastasizing have a higher rate of glucose uptake in an observed metabolic phenomenon called the Warburg effect. This increased glycolytic activity results in higher levels of intracellular lactate and has led to research in studying lactate transporters as a therapeutic target (Liberti and Locasale, 2016; Ovens et al., 2010; Tasdogan et al., 2019). Recently, in epigenetics, lactate has garnered attention because histone lysine residues have been found to be lactylated, controlling gene expression in M1 macrophages (Zhang et al., 2019). The many roles of lactate in the cell highlight the necessity of developing optimized tools to enhance the ability to measure lactate in order to better understand its role (Chen et al., 2016; Hui et al., 2017).

Despite the increasing interest and importance of lactate metabolism, methods to measure lactate dynamics *in situ* and *in vivo* are still limited (Chen et al., 2016; Hui et al., 2017). Previously, indicators have proven to be useful in metabolic studies with multiple tools developed for metabolites such as glucose and nicotinamide adenine dinucleotide (Fehr et al., 2003; Yu et al., 2019; Zhao et al., 2015). The first genetically encoded fluorescent lactate indicator, Laconic, is based on Förster resonance energy transfer (FRET) and the bacterial lactate-binding molecule LldR (San Martin et al., 2013). Laconic has been utilized in subsequent studies to better understand neuronal energetics and to identify the function of Chaski, a *Drosophila* lactate/pyruvate shuttle, as well as being the basis for MitoToxy, a screening tool for drug-induced mitochondrial toxicity (Contreras-Baeza et al., 2019; Delgado et al., 2018; Diaz-Garcia et al., 2017; Lerchundi et al., 2015; Machler et al., 2016). As a FRET sensor, however, it is limited in its ability to be used in tandem with multiple fluorescent indicators, a feature that would be of great utility given the dynamic and intertwined nature of metabolite levels. In addition, the *in vivo* studies using Laconic relied on the use of adeno-associated virus (AAV) to induce its expression, a process that is known to be immunogenic (Colella et al., 2018; Machler et al., 2016). No Laconic mouse lines are currently available. Recently, an additional lactate indicator, Green Lindoblum, was developed using an insertion of the bacterial binding molecule LldR into a loop of green fluorescent protein and is also similarly based around LldR (Harada et al., 2020). Similar to the shortcomings accompanying Laconic, this indicator has poor intracellular expression, does not have a genetically encoded *in vivo* model available, and has significantly limited lactate sensitivity, rendering precise measurements of lactate flux difficult. We sought to improve upon these lactate indicators, by utilizing molecular biological approaches and mutagenesis to develop a single fluorescent protein-based indicator built with LldR. The advances in this next-generation tool expand the ability to observe the dynamics of lactate change *in situ* and *in vivo*. The use of single fluorescence indicators enables the utilization of multiple fluorescent molecules simultaneously to monitor several metabolites or other biological events, such as calcium ion (Ca^{2+}) signaling (Germond et al., 2016; Lalonde et al., 2005; Zhang et al., 2013). The single fluorescent indicators have inherently low background signals as well as simpler detection methods compared with those necessitated by FRET-based indicators (Giepmans et al., 2006).

Here, we have developed and applied a genetically encoded metabolite indicator (GEM-IL) to study the dynamics and role of lactate in physiology and disease. Mouse *in vivo* models were developed, allowing for the cell/tissue-specific monitoring of lactate dynamics as demonstrated using isolated primary cells. In human neural progenitors, we were able to use GEM-IL to confirm the effect of c-Myc, an oncogene, which heightened lactate levels. GEM-IL can detect the effect of octyl-R-2HG, an onco-metabolite, on metabolic activity, while Laconic and Green Lindoblum could not. Altogether, we report the development and application of GEM-IL, showing its improvements on previous generations and its potential as a tool to enhance our understanding of the function and role of lactate.

RESULTS

Development of a genetically encoded metabolic indicator for lactate

A genetically encoded metabolite indicator for lactate, GEM-IL, was developed with the goal of developing a fluorescent lactate indicator that can directly measure the metabolite both *in situ* and *in vivo*. With this in mind, we aimed to select a reporter system that would be compatible with these different applications. As previously reported, superfolder fluorescent variants show improved stability, kinetics, and resistance to chemical denaturants, making them ideal fluorescent reporters for imaging lactate compared with non-superfolder fluorescent probes (Pedelacq et al., 2006; Stepanenko et al., 2014). The split version of a superfolder fluorescent protein has been used in other tools, separating the 11^{th} β strand of sfGFP ($sfGFP_{11}$) from the first 10 β strands ($sfGFP_{1–10}$) (Cabantous et al., 2005; Feng et al., 2017; Kamiyama et al., 2016). Using these strategies and designs, we tested three fluorescent proteins: superfolder cyan (sfCFP), superfolder green (sfGFP), and superfolder yellow (sfYFP). The GFP (G), YFP (Y), and CFP (C) GEM-ILs were constructed by fusing the bacterial lactate binding domain, LldR, between the 10^{th} and the 11^{th} β strands (named GEM-IL prototype). We hypothesized that the mature fluorescent molecule would undergo a conformational shift upon lactate binding to LldR, resulting in a detectable and reversible fluorescence change (Figure 1A). This is supported by the previous development of a single fluorescent indicator using conformationally sensitive GFP (csGFP) that can be conformationally manipulated by inducing

CellPress
OPEN ACCESS

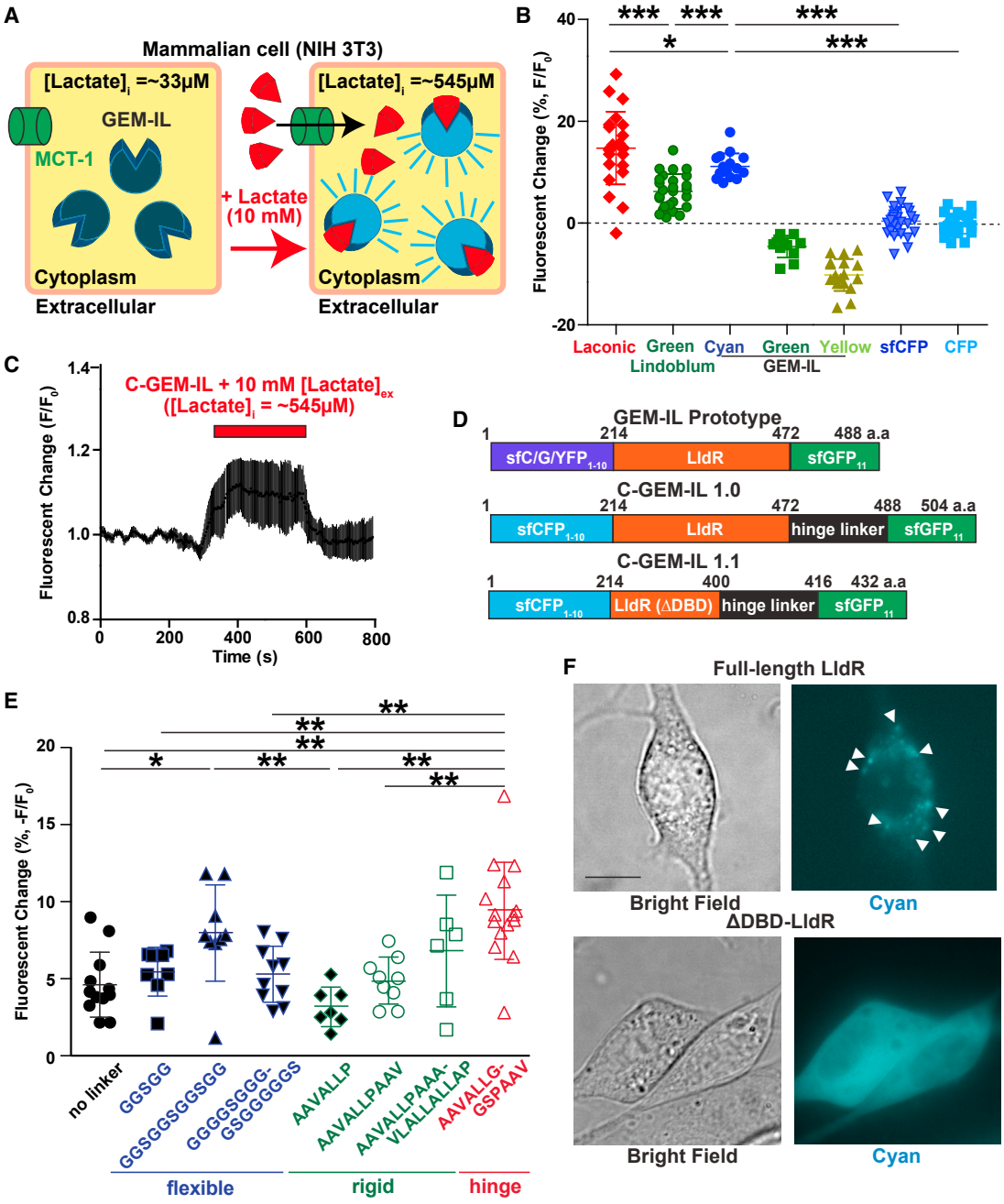

Figure 1. Development of a genetically encoded metabolic indicator for lactate (GEM-IL)

(A) Overview of the lactate indicator GEM-IL binding upon introduction of lactate.

(B) Relative fluorescence change of the cyan, green, and yellow fluorescent protein-based GEM-IL constructs after 10 mM lactate addition in NIH3T3 cells with the superfolder CFP (sfCFP), full-length cyan fluorescent protein (CFP), Laconic, and Green Lindoblum signal changes as points of comparison. Error bars represent standard deviations (n = 23, 16, 12, 18, 29, 26, and 30 samples, respectively). One-way ANOVA with multiple comparison test (Laconic versus cyan, *p = 0.0368; Laconic versus Green Lindoblum, ***p = 2.76×10^{-11}; Green Lindoblum versus cyan, ***p = 0.0008; cyan versus sfCFP, ***p = 1.58×10^{-13}; cyan versus CFP, ***p = 2.25×10^{-14}).

(C) Representative fluorescence change traces of cyan fluorescent protein-based GEM-IL (C-GEM-IL) in NIH3T3 cells.

(D) Construct maps of GEM-IL prototype, C-GEM-IL 1.0, and C-GEM-IL 1.1.

(E) Fluorescence change of G-GEM-IL with various linker types after addition of 10 mM lactate (i.e., [Lactate]i = ~545 μM according to [B]) to the imaging solution. Error bars represent standard deviations (n = 12, 8, 9, 10, 7, 9, 6, and 15, respectively). One-way ANOVA with multiple comparison tests (*p < 0.05, **p < 0.01) was used.

(F) Cyan fluorescence and bright-field images of C-GEM-IL full-length and C-GEM-IL ΔDBD in NIH3T3 cells. Arrowheads indicate the puncta seen when overexpressing C-GEM-IL. Scale bar, 10 μm.

strain on the molecule (Bonnot et al., 2014; Ganim and Rief, 2017). As expected through the known excitation and emission spectra of each fluorescent protein, we observed cyan and green fluorescence when expressing C-GEM-IL in mammalian (HEK 293T and NIH3T3) cells, as well as green and yellow fluorescence from G-GEM-IL and Y-GEM-IL (Figure S1A) (Shaner et al., 2005). The ability of GEM-IL to detect a change in lactate levels *in situ* was then assessed through the exogenous administration of 10 mM sodium lactate. This concentration is physiologically relevant, as circulating levels can range from 0.5 to 2.0 mM and even up to 40 mM after exercise or in tumor microenvironments (Goodwin et al., 2007; Walenta et al., 2000). This exogenous 10 mM administration led to an increase in cellular cytoplasmic levels from 33 ± 12 to 545 ± 149 μM (Figure S1B). Importantly, this increase in cytoplasmic lactate has no effect on the innate fluorescence of cyan fluorescent protein, suggesting that any fluorescence changes we see moving forward are the result of our lactate indicator (Figures 1B and S1C) (Proia et al., 2016). Looking to now test our indicator's response to this exogenous lactate addition, we observed that C-GEM-IL had a greater absolute fluorescence change compared with G-GEM-IL and Y-GEM-IL, with signal changes of 11.1% ± 2.5%, 4.6% ± 2.1%, and 10.2% ± 3.1%, respectively. Compared with previously developed indicators, these fluorescence changes were less than those observed using the FRET type, Laconic, but greater than Green Lindoblum (Figures 1B and 1C). We also used a full-length sfCFP molecule with no lactate binding domain as an additional control and found a signal change of only 0.38% ± 2.75%, suggesting minimal non-specific effects of the lactate addition on the fluorescent signal in live mammalian cells (Figures 1B and S1C). In addition, the binding of lactate to C-GEM-IL resulted in an increase in the fluorescent signal, which was the inverse of what is seen with G- and Y-GEM-IL. Although the exact mechanism behind this inversion is unknown, it is consistent with previous studies using csGFP (Bonnot et al., 2014). In parallel with the fluorescent protein comparisons, we tested the use of various linkers—flexible, rigid, and hinge—to better optimize our indicator given the importance of spatial constraints with superfolded fluorescent proteins. Using the green fluorescent type, G-GEM-IL, as the template, which as previously stated originally had a fluorescence change of 4.6%, we observed that adding a hinge linker between LldR and $sfGFP_{11}$ increased the absolute fluorescence change of G-GEM-IL to 9.4% ± 4.3% (Figures 1D and 1E). We integrated this improvement into our most promising fluorophore, cyan, and added a hinge linker to develop C-GEM-IL 1.0 (Figure 1D).

Furthermore, we found that C-GEM-IL 1.0 formed prominent puncta when expressed in NIH3T3 cells (Figure 1F). This may be evidence of protein aggregation brought on by poor indicator stability and folding. To alleviate this, we deleted the DNA binding domain of the LldR portion of our indicator (ΔDBD), and designated it as C-GEM-IL 1.1 (Figure 1D). The deletion eradicated the previously seen puncta, resulting in a uniform distribution of the indicator in the cytoplasm, and increased the response of this indicator to lactate perfusion to 18.3% ± 3.5%, significantly greater than that of the C-GEM-IL 1.0's 4.5% change (Figures 1F and S1D).

Fluorophore mutagenesis in C-GEM-IL

Investigating the cause behind the aforementioned inversion of fluorescence changes between C-GEM-IL and Y/G-GEM-IL, we aligned the amino acid sequences of the fluorescent proteins and found that sfCFP alone had an isoleucine at the 146^{th} position compared with an asparagine in the other proteins (Figures 1B, 2A, and S2). Suspecting this amino acid to be the cause of the positive C-GEMI-IL response to lactate, we generated an I146N mutant of C-GEM-IL 1.1 (Figure 2B). Interestingly, this did not lead to an inversion of the fluorescence change. Instead, the I146N mutation significantly enhanced the fluorescence change of C-GEM-IL 1.1 in response to lactate to 24.4% ± 10.1% (Figure 2C), leading to an improved version: C-GEM-IL 2.0. This observed change may be due to differences in the folding of mature superfolder fluorescence proteins affecting how I146 acts in relation to the chromophore compared with regular CFP. This finding is noteworthy, as in regular CFP it was previously found that the I146N mutation leads to a decrease in fluorescence (Heim and Tsien, 1996; Kubala et al., 2010; Lelimousin et al., 2009).

To further characterize our lactate indicator, we used a bacterial pCold expression system to obtain and characterize purified recombinant C-GEM-IL 2.0 protein. All recombinant protein experiments were conducted in solutions calibrated by a pH meter and confirmed stable at pH 7 unless otherwise indicated. Characteristic of CFP, we found that when excited at 425 nm, the emission spectrum remained as a single peak with a maximum emission of 490 nm (Figure 2D). The dissociation constant of the indicator (K_D) was found to be 2.33 ± 0.61 mM (Figure 2E). Measuring the response of the *in vitro* recombinant protein to various metabolites, C-GEM-IL 2.0 showed a specificity for lactate reflected in a 41.1% ± 17.5% fluorescence change, with no significant changes observed in the presence of other metabolites (Figure 2F). Although non-significant, the indicator's *in vitro* fluorescence changes in response to glucose, pyruvate, and acetate were at levels of 15.3% ± 4.0%, 16.0% ± 8.9%, and 17.2% ± 6.1%, respectively (Figure 2F), suggesting that the substrate specificity may be a concern with the current iteration of our C-GEM-IL 2.0 construct. C-GEM-IL 2.0 had comparable substrate specificity in comparison to Green Lindoblum and Laconic, which both showed minimal non-specific signaling (Harada et al., 2020; San Martin et al., 2013).

Lactate binding domain characterization and mutagenesis in C-GEM-IL

To improve upon the specificity of our indicator, we sought to identify the conserved regions or amino acids critical for lactate binding. To do so, we aligned the amino acid sequences of the lactate binding domains from three organisms: *Escherichia coli*, *Pseudomonas aeruginosa*, and *Corynebacterium glutamicum* (Figure S3A). From this alignment and computational prediction tools, SWISS-MODEL and I-TASSER, several conserved residues were targeted for mutagenesis to improve binding affinity and further optimize C-GEM-IL 2.0 (Figures 3A, 3B, and S3B). Of the candidate mutants tested, the E103D mutation resulted in the largest increase in fluorescence of 42.9% ± 9.3% in response to lactate (Figure 3B). This improvement from the 24.4% ± 10.1% change observed with C-GEM-IL 2.0 led to the development of C-GEM-IL 3.0 (Figure 3C). In addition, the mutation studies

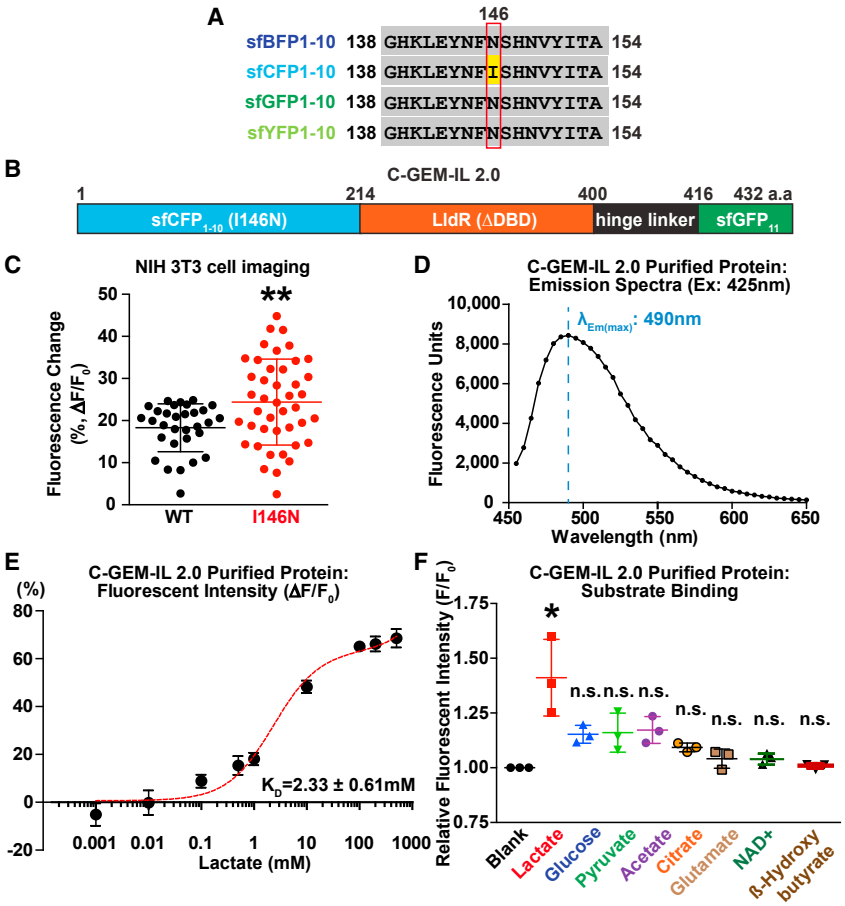

Figure 2. Fluorophore point mutation improves response to lactate

(A) Amino acid sequence alignment showing the inclusion of the I146N mutation (red outline) in C-GEM-IL (gray, a match; yellow, a mismatch).

(B) C-GEM-IL 2.0 construct map.

(C) Fluorescence intensity changes of the wild-type (WT) and I146N mutant in NIH3T3 cells. Error bars represent standard deviations (n = 31 and 43 traces, using unpaired t test, **p < 0.01).

(D) Emission spectra of recombinant C-GEM-IL 2.0 proteins purified from bacterial expression system.

(E) Lactate binding curve of the purified recombinant C-GEM-IL 2.0 protein. The non-linear curve fit for total binding used to calculate dissociation constant is shown (red).

(F) Substrate binding tests of the recombinant C-GEM-IL 2.0 protein with each substrate at 10 mM. Error bars represent standard deviations (pH 7.0, n = 3, using one-way ANOVA with multiple comparisons tests to control column [blank], *p < 0.05; n.s., no other significant differences among the groups).

included a non-responsive form of the indicator, with the H151M substitution effectively abolishing the indicator's response to lactate, with a 2.2% ± 4.2% fluorescence change (Figure 3B). This result suggests that the H151 residue is important for LldR protein activity, possibly affecting oligomerization and/or lactate binding. For our studies, this construct is useful as a negative control as fluorescent signals are often affected by a variety of factors, such as temperature, ion concentration, and pH (Aguilera et al., 2008). The importance of this residue has been similarly identified by the Laconic developer group (San Martin et al., 2013), which used an H151D mutation to generate their own "dead" indicator (available as Addgene plasmid 118627; unpublished data).

Looking more at the metabolic pathways and activity in cells, we examined whether the fluorescence change of C-GEM-IL 3.0 is in response to the influx of lactate through monocarboxylate transporter 1 (MCT1, a predominant lactate uptake pathway). NIH3T3 cells were treated with lactate in the presence or absence of AR-C155858, an MCT1 inhibitor, which inhibits the influx of lactate into the cell (Figure 3D) (Ovens et al., 2010). Following exposure of NIH3T3 cells to AR-C155858, C-GEM-IL 3.0 fluorescence did not change significantly (Figure 3E), evidencing that the fluorescence change observed is due to the MCT1-mediated lactate influx. To test whether C-GEM-IL 3.0 can detect an endogenous increase in lactate produced through glycolysis, we provided cells preconditioned in a glucose-free medium with either glucose or 2-deoxy-D-glucose (2DG). 2DG is a non-metabolizable glucose analog and thus would not lead to an increase in endogenous lactate (Figure 3F). NIH3T3 cells expressing C-GEM-IL 3.0 under these conditions could detect the change in lactate levels presumably produced through glycolysis, with a fluorescence change of 12.0% ± 4.1%, while the fluorescence change in response to 2DG was not different from baseline (Figures 3F and 3G). Confirming that this response is the result of glycolysis, we perfused glucose after the cells were exposed to AR-C155858 and observed a similar increase in fluorescence, 10.3% ± 4.4% (Figures 3F and 3G).

Again, to further characterize our most optimized indicator, the bacterial recombinant protein was purified and imaged using a Coomassie brilliant blue stain evidencing a single band at ~50 kDa representing C-GEM-IL 3.0 (Figures 3H and S3C). The recombinant protein has a single emission peak with a maximum intensity at 490 nm (Figure 3I). To investigate whether C-GEM-IL 3.0 had multiple oligomerization states, size-exclusion chromatography-based high-performance liquid chromatography (HPLC) was conducted using the purified protein, and we found that the recombinant proteins showed a single peak (Figure S3D). Of note, there is a noticeable shoulder peak in the HPLC data that accumulates after multiple freeze/thaw cycles, suggesting possible aggregation of the purified recombinant proteins. In comparison to C-GEM-IL 2.0, whose K_D was 2.33 mM, C-GEM-IL 3.0 had an improved *in vitro* K_D of 661 ± 142 μM (Figures 2E and 3J). The bacterial recombinant form of C-GEM-IL 3.0 also displayed increased specificity for lactate compared with C-GEM-IL 2.0, with a significant 87.5% ± 19.2% change in response to lactate, and an insignificant response to other metabolites (Figures 2F and 3K).

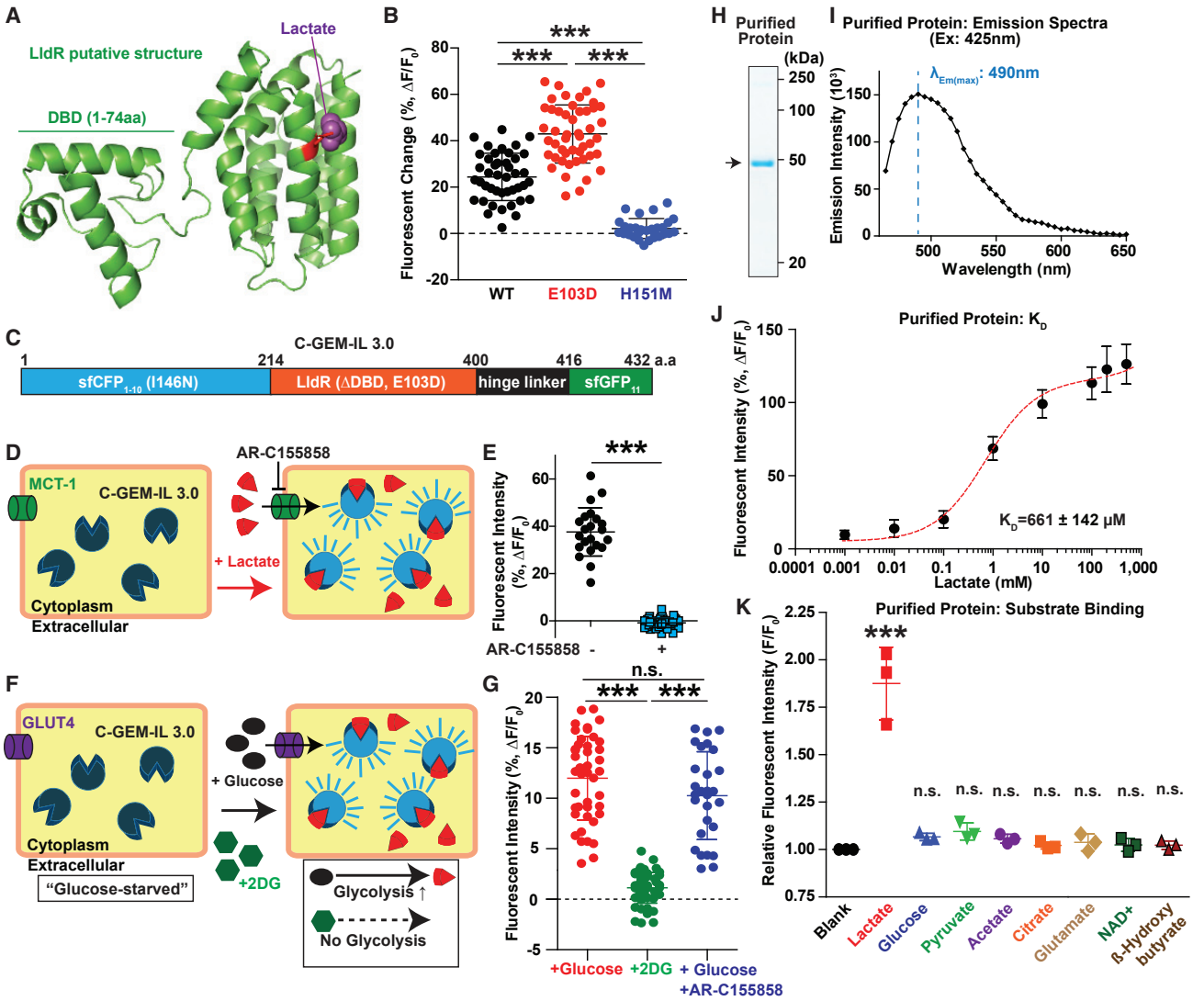

Figure 3. Mutation in lactate binding domain improves response and specificity to lactate

(A) Model of the LldR structure with the predicted lactate binding site (purple) and E103 (red).

(B) Effects of targeted amino acid substitutions E103D and H151M in the lactate binding domain on lactate-induced fluorescence of C-GEM-IL 2.0 in NIH3T3 cells. Error bars represent standard deviations (n = 63 and 37). One-way ANOVA using Dunnett's multiple comparison tests was used with wild -type (WT; ***$p < 0.001$).

(C) C-GEM-IL 3.0 construct map.

(D) Overview of C-GEM-IL binding upon introduction of lactate and the effect of AR-C155858 (MCT1 inhibitor).

(E) Fluorescence intensity changes of C-GEM-IL 3.0 and its response to 10 mM lactate addition with (black) and without treatment with AR-C155858 (100 nM, blue). Student's t test was used (***$p < 0.001$).

(F) Schematic representation of C-GEM-IL lactate sensing upon introduction of glucose after NIH3T3 cells are glucose -starved.

(G) Average fluorescence intensity changes of C-GEM-IL 3.0 and its response to glucose (10 mM) in the absence and presence of 100 nM AR-C155858 (red and blue, respectively) and a non-metabolizable glucose analog, 2DG (10 mM; green). Before glucose or 2DG was added, the cells were kept in glucose-free Tyrode's solution. Error bars represent standard deviations. One-way ANOVA with multiple comparisons test (***$p < 0.001$).

(H) Image of SDS-PAGE gel of purified recombinant C-GEM-IL 3.0 proteins (arrow).

(I) Emission spectrum of the purified recombinant proteins of C-GEM-IL 3.0.

(J) Lactate binding curve of the purified recombinant C-GEM-IL 3.0 proteins. The non-linear curve fit for total binding used to calculate the dissociation constant is shown (red).

(K) Substrate binding test of the recombinant C-GEM-IL 3.0 with each substrate at 10 mM. Error bars represent standard deviations (n = 3, using one-way ANOVA with multiple comparisons test, ***$p < 0.001$; n.s., no other significant differences among the groups).

As previously mentioned, the amount of lactate to which C-GEM-IL 3.0 is exposed in the cells is not the same as the lactate concentration in the external bath solution (Figure S1B). Taking this into account, the internal lactate concentration was measured in non-transfected NIH3T3 cells after exposure to 0–100 mM lactate using a biochemical assay (Figure S3E and S3F). The internal concentrations were then used to determine the *in situ* response and K_D of C-GEM-IL 3.0. The *in situ* K_D of C-GEM-IL 3.0 was found to be 515 ± 167 μM, similar to what was found *in vitro* using the recombinant proteins (Figures 3J and S3G).

As seen with other fluorescence-based systems, the overall fluorescence intensity of recombinant C-GEM-IL 3.0 proteins was found to shift in relation to the pH of the solution (Figure S3H) (San Martin et al., 2013). To examine whether this feature would affect our indicator's change in response to lactate, C-GEM-IL 3.0 was exposed to 0 or 10 mM lactate at pH 6.5. At this altered pH, C-GEM-IL fluorescence increased by 51.5% ± 31.7% in response to lactate (Figure S3I). To assess whether the fluorescence change seen *in situ* in NIH3T3 cells was affected by a change in intracellular pH caused by the lactate infusion, the response of the recombinant form of the indicator was measured after exposure to 30 or 500 μM lactate, levels meant to mimic the increase in cytoplasmic lactate observed with a 10 mM exogenous addition of lactate *in situ* (Figure S1B). This led to a 37.8% ± 11.8% and 40.7% ± 17.0% increase in the recombinant protein fluorescence purified from bacterial and mammalian cells (HEK 293T), respectively (Figure S3J). This *in vitro* change is consistent with what is observed in NIH3T3 live cells *in situ* (a 42.9% increase), evidencing that the fluorescence increase can reliably be attributed to lactate binding to C-GEM-IL 3.0. Following a previous study identifying a pH-stable GFP variant (Roberts et al., 2016), a pH-insensitive mutant of C-GEM-IL 3.0, named C-GEM-IL 3.0p (N149Y/Q204H), was developed. In response to 10 mM exogenous lactate addition, this mutation led to a fluorescence change of 21.7% ± 4.2% *in situ*, a significant decrease compared with C-GEM-IL 3.0 (Figure S3K). Importantly, however, the purified recombinant form of C-GEM-IL 3.0p still showed a specific significant response to lactate with no significant change in the fluorescence of the sensor in response to the other metabolites (Figure S3L).

Comparison of C-GEM-IL 3.0, Laconic, and Green Lindoblum

The aim of this study is to develop an improved lactate indicator to enable more researchers to better measure lactate changes. The previously developed genetically encoded lactate sensors, Laconic and Green Lindoblum, have been utilized in various studies but have certain characteristics that may limit their use. C-GEM-IL 3.0 improves upon these indicators in several significant ways. The first is that C-GEM-IL 3.0 does not have low signal expression or form puncta when genetically overexpressed in NIH3T3 cells, which was observed with Laconic, Green Lindoblum, and C-GEM-IL 1.0 (Figures 1F and 4A). The next is that C-GEM-IL 3.0 has significantly improved response to lactate compared with Green Lindoblum (42.9% versus 6.2%, respectively, Figures 1B and 3E). Furthermore, C-GEM-IL 2.0 and 3.0 are capable of measuring the production of lactate generated via glycolysis, while Laconic and Green Lindoblum could not (responses of 4.5 ± 1.2, 12.0 ± 4.1, −1.1 ± 3.8, and 1.8 ± 1.2%, respectively, Figure 4B). In looking more at the protein expression of the different indicators, the C-GEM-IL series shows a single band on Western blotting compared with the dual unidentified bands seen with Laconic, suggesting that the Laconic construct may be degraded/truncated and/or cleaved, and the fluorescence change of Laconic might not be reliable (Figure 4C). Lastly, in an attempt to simply improve upon the currently available indicators, we looked to see whether any of the alterations conducted in C-GEM-IL development would be applicable for Laconic, and prepared E103D, ΔDBD/E103D, and H151D versions of the Laconic indicator. None of these changes improved the fluorescence response observed, and each of these changes led to a significantly less responsive form for the sensor, with FRET changes of 6.5% ± 1.1%, 6.2% ± 0.7%, and 5.5% ± 2.0% in response to lactate *in situ*, respectively (Figure 4D). In addition, in comparing the non-functional "dead" version of our indicator, H151M C-GEM-IL, to H151D Laconic, we found that H151M C-GEM-IL had a signal closer to baseline, with observed responses of 2.2% and 5.5%, respectively (Figures 3B and 4D). Overall, C-GEM-IL 3.0 improves on the currently available indicators, and offers a more precise and reliable method for measuring lactate changes in live cells compared with Laconic and Green Lindoblum (Figure 4D; Box 1C).

Ratiometric versions of C-GEM-IL 3.0

Although C-GEM-IL 3.0 is useful in the detection of lactate as a single-fluorophore-based indicator (Figure S4A), it does not allow for the exact quantification of lactate due to factors extrinsic to the stimulant (Grynkiewicz et al., 1985; Paredes et al., 2008). Adding a ratiometric version of GEM-IL improves sensitivity through an internal reference and allows for quantitative analysis, should users of this tool prefer such capabilities or have experimental setups that support this version (Lee et al., 2015). Therefore, we developed a ratiometric version of C-GEM-IL 3.0 by adding a secondary fluorescent molecule (either YFP or red fluorescent protein, RFP) with the fluorescent indicator after a linker (Figure S4B). Interrogating the expression of appending YFP to C-GEM-IL 3.0 through Western blotting showed a single band at 75 kDa (Figures S4B–S4D). Linking a YFP to C-GEM-IL 3.0 through either an Ala-Ser (AS) or a rigid linker rendered the mature CFP unresponsive to lactate, while the YFP signal decreased, possibly a FRET change of 29.7% ± 5.7% and 16.0% ± 4.4%, respectively (Figures S4E and S4F). Examining alternative fluorophores to append, we used a rigid linker to add an RFP, mKate2 or mCherry, to the carboxyl terminus of C-GEM-IL 3.0. Expression of these constructs led to two bands between 50 and 75 kDa on western blotting due to an unknown degradation/truncation mechanism as observed in Laconic (Figures 4C, S4C, and S4D). This possible degradation/truncation suggests a potentially unstable biosensor, so as an alternative approach to address this concern, we applied a self-cleaving peptide P2A sequence, generating C-GEM-IL 3.0r (Figure S4G) (Kawano et al., 2016; Kim et al., 2011). The P2A

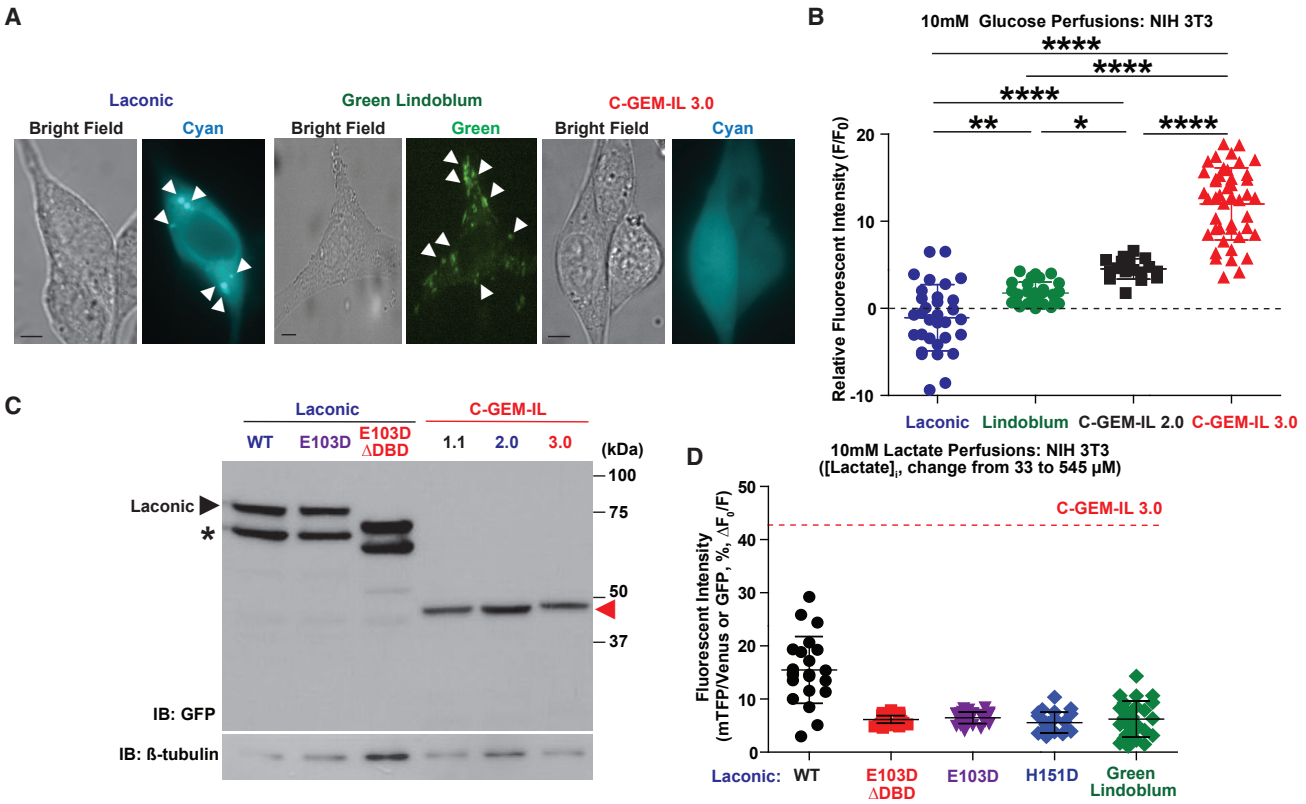

Figure 4. Comparison of C-GEM-IL, Laconic, and Green Lindoblum

(A) Representative cyan/green fluorescence and bright-field images of NIH3T3 cells expressing Laconic, Green Lindoblum, and C-GEM-IL 3.0 (scale bar, 5 μm). White arrowheads shown highlighting puntae formation

(B) Fluorescence change of Laconic (mTFP/Venus), Green Lindoblum, and C-GEM-IL 2.0 and 3.0 (cyan) in response to 10 mM glucose perfusions to glucose-starved NIH3T3 cells. The experimental design is identical to the one conducted in Figure 3F (n = 32, 30, 17, and 45 traces, respectively, using one-way ANOVA with multiple comparisons test, *p < 0.05, **p < 0.01, ****p < 0.001).

(C) Anti-GFP Western blot results interrogating the expression of the various iterations of Laconic and C-GEM-IL expressed in NIH3T3 cells. Arrowheads show Laconic (black) and C-GEM-IL proteins (red). *Truncated Laconic proteins. β-tubulin, a housekeeping molecule, was also tested as a reference.

(D) Fluorescence change of various iterations of Laconic and Green Lindoblum in response to the exposure of NIH3T3 cells to 10 mM lactate. Red dashed line represents the average fluorescence change observed with C-GEM-IL 3.0. Error bars represent standard deviations (n = 22, 51, 33, 22, and 26).

cleavage was not fully efficient, with bands at 75 kDa (non-cleaved, ~10%) and 50 kDa (cleaved, ~90%) (Figure S4H). Of note, there was a band evident between 50 and 60 kDa potentially due to the truncation of the non-cleaved proteins. NIH3T3 cells transfected with C-GEM-IL 3.0r responded to lactate exposure *in situ*, with the cyan signal changing in reference to the mKate2 fluorophore. We observed the fluorescence change of this indicator at increasing levels of lactate to generate a linear-regression-based model for lactate quantitation (Figure S4I). Using this model, we calculated that the observed change in fluorescent signal, which had a ratiometric response of 30.0% ± 6.5%, could be equilibrated to an internal lactate increase of 622 μM (Figure S4J). Also, the mKate2 signal remained constant during lactate addition and binding, again evidencing the resistance of fluorescent molecules to cellular changes due to lactate influx into the cells, as also observed in CFP and sfCFP (Figures 1B and S1C). This version of our indicator can be valuable in future applications to determine the amount of lactate generated from other metabolites and/or biological processes.

Applications of C-GEM-IL for lactate imaging with octyl-R-2HG and c-Myc

We then sought to examine the utility of our most optimized indicator, C-GEM-IL 3.0, in observing lactate changes in other applications and settings. Octyl-R-2HG, a membrane-permeative precursor of D-2-hydroxyglutarate, is an onco-metabolite that inhibits ATP synthase and mTOR signaling (Fu et al., 2015). Increasing levels of D-2-hydroxyglutarate were found to increase the levels of lactate (Bottcher et al., 2018). To determine whether C-GEM-IL 3.0 could detect a change in lactate levels in response to this substrate, NIH3T3 cells were treated with octyl-R-2HG. It was found that addition of octyl-R-2HG led to a detectable fluorescence increase of C-GEM-IL 3.0 by lactate of 27.9% ± 8.0% in these cells (Figure 5A), demonstrating the indicator's ability to respond to changes in cellular metabolism elicited by chemical stimulants. Laconic and Green Lindoblum, on the other hand, were unable to detect this change in metabolism, with fluorescence changes of 2.8% ± 2.0% and 5.0% ± 3.0%, respectively (Figure 5A).

CellPress
OPEN ACCESS

Box 1. Summary of GEM-IL development and comparison of Laconic, Green Lindoblum, and GEM-IL lactate indicators

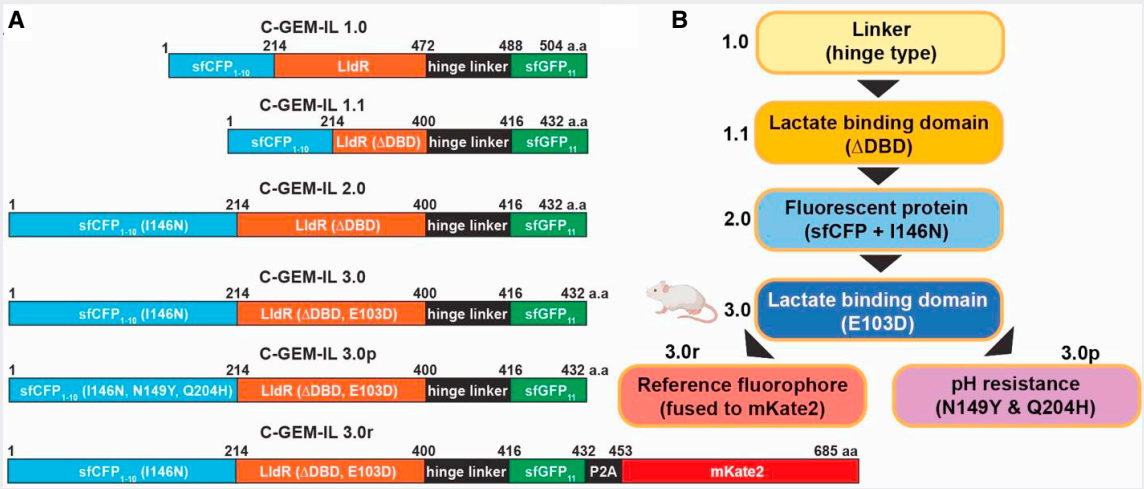

C

	Laconic	Green Lindoblum	GEM-IL
Indicator Size	83.8 kDa	60 kDa	48.5 kDa
Available Flurophores	FRET (mTFP/Venus)	GFP	various fluorescent protein (sfCFP, sfGFP & sfYFP)
Response to 10mM Lactate (*in vitro*, NIH 3T3 cells)	~15%	~6%	~40%
Substrate Specificity	O	O	O
Detects Metabolic Activity (glucose, drug metabolism & cancer metabolism)	-	-	O
in vivo Mouse Model Availability	-	-	O
Expression Pattern in Live Mammalian Cells (ex. NIH 3T3)	Aggregated	Aggregated & low expression	Uniform in the cytoplasm
KD	8 μM / 830 μM (San Martin, 2013)	3mM (Harada, 2020)	661 ± 142μM
pH-insensitive Construct Availability	-	-	O
Quantification Reliability	High (FRET)	Medium (single fluorescent)	Medium (single fluorescent)
Dual Imaging Capability	-	O	O

(A) Construct maps of each GEM-IL iteration, detailing the changes made in each and in which particular domains the modifications were made.
(B) Flow chart highlighting the major modification in each construct. Mouse model is available for C-GEM-IL 3.
(C) Comparison table of Laconic, Green Lindoblum, and GEM-IL indicators.

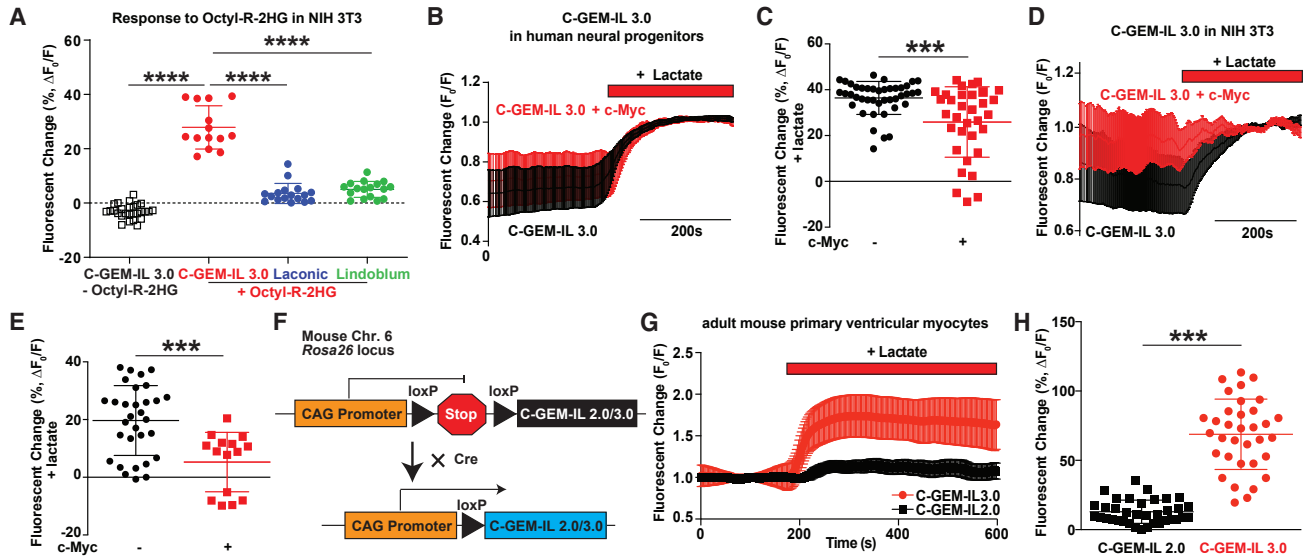

Figure 5. Applications of C-GEM indicators

(A) Quantification of the average fluorescence changes of C-GEM-IL 3.0, Laconic, and Green Lindoblum in NIH3T3 cells upon exposure to 1 mM octyl-R-2HG. Error bars represent standard deviations (n = 27, 14, 17, and 17 samples in three independent experiments, one-way ANOVA with multiple comparisons, ****$p < 0.0001$).

(B) Cumulative trace overlay of c-Myc-infected and non-infected human neural progenitors upon addition of 10 mM lactate to imaging solution. Error bars represent standard deviations (n = 46 and 31 traces in two independent experiments).

(C) C-GEM-IL 3.0 fluorescence changes in c-Myc-infected human neuronal progenitors. Error bars represent standard deviations (n = 46 and 31 traces in two independent experiments, using unpaired two-tailed t test with Welch's correction, ***$p < 0.001$).

(D) Cumulative trace overlay of c-Myc-infected and non-infected NIH3T3 cells upon addition of 10 mM lactate. Error bars represent standard deviations.

(E) Fluorescence changes in c-Myc-infected NIH3T3 cells and controls. Error bars represent standard deviations (n = 31 and 15 samples, using unpaired two-tailed Student's t test with Welch's correction, ***$p < 0.001$).

(F) Simplified diagram showing the insertion of the C-GEM-IL 2.0 or 3.0 indicator into mouse *Rosa26* locus and the effect of crossing with a Cre line.

(G) Cumulative traces showing the extracellular lactate-induced fluorescence increase in adult ventricular myocytes isolated from C-GEM-IL 2.0 and 3.0 mice crossed with cardiac Cre drivers. Error bars represent standard deviations.

(H) Quantification of the fluorescence changes upon introduction of 10 mM lactate in the imaging solution to the cardiomyocytes isolated from C-GEM-IL 2.0- and 3.0-expressing mice. Error bars represent standard deviations (n = 36 and 34 traces, respectively, using unpaired two-tailed t test with Welch's correction, ***$p < 0.001$).

Overexpression of c-Myc, an oncogene, has been shown to alter the metabolic state of cells with an increased need to support cellular proliferation accompanied by an increase in lactate production (Miller et al., 2012). To assess if our indicator can detect this shift in cellular profiles, we virally overexpressed c-Myc in NIH3T3 cells and human neuronal progenitors derived from induced pluripotent stem cells (iPSCs) as a model of a central nervous system primitive neuro-ectodermal tumor (CNS-PNET) (Behdad and Perry, 2010). In this model, c-Myc overexpression results in a heightened level of lactate production in the cellular environment. Here we found that the addition of lactate to these c-Myc-infected oncogenic cells resulted in a smaller fluorescence change of our indicator compared with non-infected cells, showing that the indicator can distinguish between the two metabolic states (Figures 5B–5E). The lower response seen in the oncogenic cells could be due to the heightened metabolic state induced by increased c-Myc expression, resulting in significantly higher endogenous lactate concentrations compared with non-infected controls, which was supported by a lactate biochemical assay of the cell lysate and culture medium (Figures S5A–S5C). The higher basal lactate levels would result in a higher baseline fluorescence of our indicator, so any further lactate addition would not result in as large of an increase in fluorescence.

Simultaneous imaging of lactate and calcium ion

To further demonstrate the possibility of simultaneous fluorescence imaging using C-GEM-IL 3.0, we conducted live cell imaging for lactate and Ca^{2+} using C-GEM-IL 3.0 and R-GECO1, a genetically encoded red fluorescent Ca^{2+} indicator (Zhao et al., 2011). We found that the cytoplasmic Ca^{2+} levels significantly decreased with the increase in lactate in the cells (Figures S5D and S5E). This finding further evidences that GEM-IL can be used in tandem with other indicators, even those that monitor metabolites from traditionally unassociated metabolic pathways. This will allow for the examination of the effects of various chemicals and metabolites and how they relate to varying levels in lactate.

Generation of C-GEM-IL mouse lines

Rather critically, the measurement of lactate in organs and tissue relies on indirect measurements, including the use of electrodes measuring extracellular lactate or radioisotope-labeled metabolites coupled with mass spectrometry, effectively

allowing for only snapshots of lactate handling (Marzouk et al., 2002; Sugiura et al., 2016). An improved *in vivo* model would be invaluable to study lactate dynamics in healthy and disease models. In cardiac physiology, for example, an increase in the serum level of lactate correlates negatively with patient survival after heart failure (Hattori et al., 1985; Kawase et al., 2015). To enable the monitoring of lactate levels during normal physiology and disease, *in vivo* mouse models expressing either C-GEM-IL 2.0 or C-GEM-IL 3.0 were generated by inserting either version of the indicator into the *Rosa26* locus (Rosa26-Cag-lox-stop-lox-C-GEM-IL, Figures 5F and S5F). The C-GEM-IL mouse models were used to induce the expression of either indicator in cardiac tissue by crossing the C-GEM-IL 2.0 and 3.0 mouse lines with either a tamoxifen-inducible α-myosin heavy chain promoter-driven Cre-expression mouse (αMHC/Myh6-MerCreMer/Cre^{ERT}), which restricts the indicator expression to the heart in response to tamoxifen, or a non-inducible-type, αMHC-Cre, mouse, respectively (Sohal et al., 2001). The expression was confirmed through PCR showing Cre-loxP recombination specifically in cardiac tissue, and the expression of C-GEM-IL 2.0 and 3.0 was further confirmed by Western blotting; furthermore, Cre transient expression could also induce C-GEM-IL 3.0 protein expression in other tissues, such as liver (Figures S5F–S5K). The overexpression of the indicator did not deleteriously affect the architecture of the mouse hearts as evidenced by the echocardiograms (Figure S5L). To confirm the functionality, we isolated adult primary cardiomyocytes from C-GEM-IL 2.0 and 3.0 mice and observed the changes in fluorescence after lactate exposure. C-GEM-IL 3.0 cardiomyocytes had a significantly higher response of 68.8% ± 4.3% compared with the 12.9% ± 1.4% change observed with the 2.0 version, confirming the successful generation and validation of our mouse lines (Figures 5G, 5H, and S5M).

DISCUSSION

This work describes the development and applications of C-GEM-IL 3.0, a single superfolder fluorescent protein-based indicator with a mutation, E103D, which improves upon the previously available lactate indicators, Laconic and Green Lindoblum. The novel design of GEM-IL generated uniform cytoplasmic expression and improved sensitivity and response, and allowed for the successful generation of a genetically encoded *in vivo* mouse model with greater ease of use in various fields (Box 1A and 1B). The benchmark experiments in this study using Laconic and Green Lindoblum proved them to either be poorly expressed or have possible putative truncated forms (Figures 4A and 4C), suggesting that the responses from these indicators might not reflect lactate concentration precisely and that the experimental outcomes and conclusions from the previous literatures could be unsure (Contreras-Baeza et al., 2019; Delgado et al., 2018; Diaz-Garcia et al., 2017; Lerchundi et al., 2015; Machler et al., 2016). Direct comparisons highlight the improvements in the GEM-IL series (Box 1C).

The development of C-GEM-IL involved multiple iterations (Box 1A and 1B). C-GEM-IL 1.0 was a functional prototype that had a 4.5% fluorescence change and formed puncta when expressed *in situ* in live mammalian cells. The removal of the DNA binding domain (C-GEM-IL 1.1) alleviated the puncta seen. Two mutations to the sensor, I146N in the sfCFP portion as well as E103D in the LldR, subsequently increased the lactate sensitivity of C-GEM-IL, making versions 2.0 and 3.0, respectively. C-GEM-IL 2.0 and 3.0 were significant improvements with fluorescent responses to lactate of 24.4% and 42.9% compared with the original FRET-based type, Laconic, which evidenced a 15.5% change, and Green Lindoblum, which had only a 6.2% change in 10 mM lactate perfusion. Importantly, the E103D mutant improved the lactate specificity of the indicator, and possibly suggests importance for this residue in LldR function. However, further development is required to generate GEM-IL series with varying kinetics and expression to targeted subcellular organelles such as the nucleus, plasma membrane, mitochondria, and endoplasmic reticulum. To this point, the pH-stable and ratiometric versions, C-GEM-IL 3.0p and 3.0r, can be useful to increase potential applications of fluorescent lactate imaging. Unfortunately, the pH-insensitive version, 3.0p, had significantly lower fluorescent response to lactate. The two point mutations (N149Y and Q204H) used to generate a pH-insensitive version appear to have also decreased the sensor's overall sensitivity to lactate. This is supported by the recombinant protein data, which were collected at a stable pH 7 and showed that 3.0p still has a significant sensitivity to lactate but lower than that of the original C-GEM-IL 3.0. Control perfusion experiments using just the fluorophores to examine whether lactate addition can change the fluorescent signals in live mammalian cells showed that neither CFP not sfCFP had any significant/obvious changes in signal when 10 mM lactate was added to the imaging solution (Figures 1B and S1C). While fluorescent proteins are known to be pH sensitive, the lactate perfusion to live cells does not affect the fluorescent signal of CFP and sfCFP in the live cells. A benefit of developing a single fluorescence indicator is the ability to use multiple fluorescent sensors at the same time to measure different probes and reporters. As evidence of this, C-GEM-IL 3.0 was successfully used in tandem with R-GECO1, a Ca^{2+} red fluorescent indicator, showing a negative correlation between lactate administration and the R-GECO1 Ca^{2+} signal. The molecular mechanism underlying the effects of lactate on intracellular Ca^{2+} handling remains unclear. Investigating the association of lactate with Ca^{2+} handling is an interesting direction as a future study.

Employing C-GEM-IL 3.0 allowed us to detect the difference in lactate response of metabolically disparate cells driven by c-Myc overexpression in NIH3T3 cells and human iPSC-derived neural progenitor cells. Octyl-R-2HG led to a detectable increase in lactate in live cells, revealing the ability of C-GEM-IL 3.0 to respond to changes in cellular metabolism induced by such onco-metabolites. The other currently available indicators, Laconic and Green Lindoblum, were unable to achieve such results. Our GEM-IL can be beneficial in chemical biology study to determine the metabolic effects of various small molecules on the levels of lactate as well as being used as a screening tool to assess the utility of these compounds in biomedical research.

To enable the investigation of lactate levels *in vivo*, we developed genetically encoded mouse strains that contain a Cre-inducible cassette for the expression of either C-GEM-IL

2.0 or C-GEM-IL 3.0 by inserting the sequences into the *Rosa 26* locus. When crossed with cardiac Cre drivers such as αMHC-Cre, isolated adult primary cardiomyocytes responded to lactate perfusion, demonstrating that the indicator was expressed and functioned with C-GEM-IL 3.0, showing a significantly improved response over C-GEM-IL 2.0.

Overall, GEM-IL is a powerful tool set that allows us to obtain new insights into the roles of lactate as an essential metabolite in live cells with single-cell resolution. As this is the initial set of iterations on the indicator, future work should focus on refining the kinetics and subcellular and extracellular expression of the GEM-IL series. We hope that further development of genetically encoded fluorescent indicators, similar to C-GEM-IL, for other metabolites will be useful in biomedical applications that probe metabolic changes in both normal and disease states with single-cell resolution to better understand the importance of various metabolites in physiology and disease.

Limitations of the study

Our tool, GEM-IL, provides an additional method for monitoring lactate influx and efflux in cells. Capitalizing on the compact nature and innate characteristics of superfolder fluorescent proteins, we were able to generate a tool with stable expression, high specificity, better sensitivity, and wider-spread applicability compatible with other lactate indicators. In addition, we achieved and demonstrated *in vivo* expression and functionality in a cardiac-specific murine model. Given that this is an indicator based on a fluorescent protein, we recognize some of the limitations that accompany this feedback system, such as pH sensitivity, photobleaching, and quantitative analysis. We sought to address these issues through different iterations of GEM-IL: C-GEM-IL3.0p and C-GEM-IL3.0r. In addition, we recognize that our indicator requires an experimental setup capable of monitoring changes in cyan fluorescence. Although we believe this to be a reasonable requirement, our indicator can also be visible with green and yellow fluorescent protein filters, although the signal will not be as strong due to the close spectral properties of these proteins. Last, we acknowledge that in this study we focused on proof of principle and benchmark experiments to validate our new lactate indicators, not on biological applications, as a method report. However, the plasmid DNA, viral construct, and mouse line of GEM-IL will be widely applicable for various researchers as a new resource to investigate lactate metabolism and provide new insights into the role of lactate.

STAR★METHODS

Detailed methods are provided in the online version of this paper and include the following:

- KEY RESOURCES TABLE
- RESOURCE AVAILABILITY
  - Lead contact
  - Materials availability
  - Data and code availability
- EXPERIMENTAL MODEL AND SUBJECT DETAILS
  - Mice
  - Cell culture
- METHOD DETAILS
  - Lactate biochemical assay
  - Plasmid DNA construction
  - Lentiviral generation and infection of NPC and NIH 3T3 cells
  - Plasmid DNA transfection
  - Purification and characterization of recombinant protein
  - Fluorescent HPLC
  - Cellular perfusion experiments
  - Kinetic measurement
  - Multi-filter fluorescent imaging
  - Hydrodynamic tail vein injection
  - Echocardiographic measurements
  - Homology modelling
  - Western blotting
- QUANTIFICATION AND STATISTICAL ANALYSIS

SUPPLEMENTAL INFORMATION

Supplemental information can be found online at https://doi.org/10.1016/j.crmeth.2021.100092.

ACKNOWLEDGMENTS

We thank Luis Felipe Barros (Centro de Estudios Científicos, Valdivia, Chile), for providing the Laconic plasmid and helpful advice on the construct, and Steven O. Marx and Lin Yang (Columbia University, USA) for their helpful discussion and mouse myocyte isolation. This work was supported by the Columbia Stem Cell Initiative, ImPACT Program (The Council for Science, Technology and Innovation, CSTI, Cabinet Office, Government of Japan, Japan) and JSPS (Japan Society for the Promotion of Science, Japan), Core-to-Core Program and White Rock Foundation.

AUTHOR CONTRIBUTIONS

M.Y. conceived of and designed this project. R.B., J.R.Q., S.U., F.K., K.M., A.D.K., T.C.L., K.N., T.M.L., R.L., M.V.Y., and M.Y. designed and/or performed the experiments. S.U., F.K., and M.Y. designed constructs and performed the mutagenesis to improve the indicator constructs. C-S.L. and M.Y. conducted mouse embryonic stem cell targeting and the mouse generation. R.B., J.R.Q., T.C.L., K.M., K.N., T.L., A.C., and M.Y. analyzed the data. R.B., J.R.Q., and M.Y. interpreted the data and wrote the manuscript. F.K., S.H., A.I.S., and K.G. helped M.Y. supervise this interdisciplinary team and proofread the manuscript. All co-authors approved the manuscript.

DECLARATION OF INTERESTS

The authors declare no competing interests.

Received: April 4, 2021
Revised: July 26, 2021
Accepted: September 15, 2021
Published: October 21, 2021

REFERENCES

Adeva-Andany, M., Lopez-Ojen, M., Funcasta-Calderon, R., Ameneiros-Rodriguez, E., Donapetry-Garcia, C., Vila-Altesor, M., and Rodriguez-Seijas, J. (2014). Comprehensive review on lactate metabolism in human health. Mitochondrion *17*, 76–100.

Aguilera, L., Campos, E., Gimenez, R., Badia, J., Aguilar, J., and Baldoma, L. (2008). Dual role of LldR in regulation of the lldPRD operon, involved in L-lactate metabolism in Escherichia coli. J. Bacteriol. *190*, 2997–3005.

Baltazar, F., Afonso, J., Costa, M., and Granja, S. (2020). Lactate beyond a waste metabolite: metabolic affairs and signaling in malignancy. Front. Oncol. *10*, 231.

Behdad, A., and Perry, A. (2010). Central nervous system primitive neuroectodermal tumors: a clinicopathologic and genetic study of 33 cases. Brain Pathol. *20*, 441–450.

Bonnot, A., Guiot, E., Hepp, R., Cavellini, L., Tricoire, L., and Lambolez, B. (2014). Single-fluorophore biosensors based on conformation-sensitive GFP variants. FASEB J. *28*, 1375–1385.

Bottcher, M., Renner, K., Berger, R., Mentz, K., Thomas, S., Cardenas-Conejo, Z.E., Dettmer, K., Oefner, P.J., Mackensen, A., Kreutz, M., et al. (2018). D-2-hydroxyglutarate interferes with HIF-1alpha stability skewing T-cell metabolism towards oxidative phosphorylation and impairing Th17 polarization. Oncoimmunology *7*, e1445454.

Boumezbeur, F., Petersen, K.F., Cline, G.W., Mason, G.F., Behar, K.L., Shulman, G.I., and Rothman, D.L. (2010). The contribution of blood lactate to brain energy metabolism in humans measured by dynamic 13C nuclear magnetic resonance spectroscopy. J. Neurosci. *30*, 13983–13991.

Cabantous, S., Pedelacq, J.D., Mark, B.L., Naranjo, C., Terwilliger, T.C., and Waldo, G.S. (2005). Recent advances in GFP folding reporter and split-GFP solubility reporter technologies. Application to improving the folding and solubility of recalcitrant proteins from Mycobacterium tuberculosis. J. Struct. Funct. Genomics *6*, 113–119.

Chen, Y.J., Mahieu, N.G., Huang, X., Singh, M., Crawford, P.A., Johnson, S.L., Gross, R.W., Schaefer, J., and Patti, G.J. (2016). Lactate metabolism is associated with mammalian mitochondria. Nat. Chem. Biol. *12*, 937–943.

Colella, P., Ronzitti, G., and Mingozzi, F. (2018). Emerging issues in AAV-mediated in vivo gene therapy. Mol. Ther. Methods Clin. Dev. *8*, 87–104.

Contreras-Baeza, Y., Ceballo, S., Arce-Molina, R., Sandoval, P., Alegría, K., Barros, L.F., and San Martín, A. (2019). MitoToxy Assay: A Novel Cell-Based Method for the Assessment of Metabolic Toxicity in a Multiwell Plate Format Using a Lactate FRET Nanosensor, Laconic (bioRxiv), p. 583096.

Cortes-Campos, C., Elizondo, R., Carril, C., Martinez, F., Boric, K., Nualart, F., and Garcia-Robles, M.A. (2013). MCT2 expression and lactate influx in anorexigenic and orexigenic neurons of the arcuate nucleus. PLoS One *8*, e62532.

Delgado, M.G., Oliva, C., Lopez, E., Ibacache, A., Galaz, A., Delgado, R., Barros, L.F., and Sierralta, J. (2018). Chaski, a novel Drosophila lactate/pyruvate transporter required in glia cells for survival under nutritional stress. Sci. Rep. *8*, 1186.

Diaz-Garcia, C.M., Mongeon, R., Lahmann, C., Koveal, D., Zucker, H., and Yellen, G. (2017). Neuronal stimulation triggers neuronal glycolysis and not lactate uptake. Cell Metab. *26*, 361–374 e364.

Fehr, M., Lalonde, S., Lager, I., Wolff, M.W., and Frommer, W.B. (2003). In vivo imaging of the dynamics of glucose uptake in the cytosol of COS-7 cells by fluorescent nanosensors. J. Biol. Chem. *278*, 19127–19133.

Feng, S., Sekine, S., Pessino, V., Li, H., Leonetti, M.D., and Huang, B. (2017). Improved split fluorescent proteins for endogenous protein labeling. Nat. Commun. *8*, 370.

Fu, X., Chin, R.M., Vergnes, L., Hwang, H., Deng, G., Xing, Y., Pai, M.Y., Li, S., Ta, L., Fazlollahi, F., et al. (2015). 2-Hydroxyglutarate inhibits ATP synthase and mTOR signaling. Cell Metab. *22*, 508–515.

Ganim, Z., and Rief, M. (2017). Mechanically switching single-molecule fluorescence of GFP by unfolding and refolding. Proc. Natl. Acad. Sci. U S A *114*, 11052–11056.

Germond, A., Fujita, H., Ichimura, T., and Watanabe, T.M. (2016). Design and development of genetically encoded fluorescent sensors to monitor intracellular chemical and physical parameters. Biophys. Rev. *8*, 121–138.

Giepmans, B.N., Adams, S.R., Ellisman, M.H., and Tsien, R.Y. (2006). The fluorescent toolbox for assessing protein location and function. Science *312*, 217–224.

Goodwin, M.L., Harris, J.E., Hernandez, A., and Gladden, L.B. (2007). Blood lactate measurements and analysis during exercise: a guide for clinicians. J. Diabetes Sci. Technol. *1*, 558–569.

Grynkiewicz, G., Poenie, M., and Tsien, R.Y. (1985). A new generation of Ca2+ indicators with greatly improved fluorescence properties. J. Biol. Chem. *260*, 3440–3450.

Harada, K., Chihara, T., Hayasaka, Y., Mita, M., Takizawa, M., Ishida, K., Arai, M., Tsuno, S., Matsumoto, M., Ishihara, T., et al. (2020). Green fluorescent protein-based lactate and pyruvate indicators suitable for biochemical assays and live cell imaging. Sci. Rep. *10*, 19562.

Hattori, R., Takatsu, Y., Yui, Y., Sakaguchi, K., Susawa, T., Murakami, T., Tamaki, S., and Kawai, C. (1985). Lactate metabolism in acute myocardial infarction and its relation to regional ventricular performance. J. Am. Coll. Cardiol. *5*, 1283–1291.

Heim, R., and Tsien, R.Y. (1996). Engineering green fluorescent protein for improved brightness, longer wavelengths and fluorescence resonance energy transfer. Curr. Biol. *6*, 178–182.

Hui, S., Ghergurovich, J.M., Morscher, R.J., Jang, C., Teng, X., Lu, W., Esparza, L.A., Reya, T., Le, Z., Yanxiang Guo, J., et al. (2017). Glucose feeds the TCA cycle via circulating lactate. Nature *551*, 115–118.

Kamiyama, D., Sekine, S., Barsi-Rhyne, B., Hu, J., Chen, B., Gilbert, L.A., Ishikawa, H., Leonetti, M.D., Marshall, W.F., Weissman, J.S., et al. (2016). Versatile protein tagging in cells with split fluorescent protein. Nat. Commun. *7*, 11046.

Kawano, F., Okazaki, R., Yazawa, M., and Sato, M. (2016). A photoactivatable Cre-loxP recombination system for optogenetic genome engineering. Nat. Chem. Biol. *12*, 1059–1064.

Kawase, T., Toyofuku, M., Higashihara, T., Okubo, Y., Takahashi, L., Kagawa, Y., Yamane, K., Mito, S., Tamekiyo, H., Otsuka, M., et al. (2015). Validation of lactate level as a predictor of early mortality in acute decompensated heart failure patients who entered intensive care unit. J. Cardiol. *65*, 164–170.

Kim, J.H., Lee, S.R., Li, L.H., Park, H.J., Park, J.H., Lee, K.Y., Kim, M.K., Shin, B.A., and Choi, S.Y. (2011). High cleavage efficiency of a 2A peptide derived from porcine teschovirus-1 in human cell lines, zebrafish and mice. PLoS One *6*, e18556.

Kubala, M.H., Kovtun, O., Alexandrov, K., and Collins, B.M. (2010). Structural and thermodynamic analysis of the GFP:GFP-nanobody complex. Protein Sci. *19*, 2389–2401.

Lalonde, S., Ehrhardt, D.W., and Frommer, W.B. (2005). Shining light on signaling and metabolic networks by genetically encoded biosensors. Curr. Opin. Plant Biol. *8*, 574–581.

Lee, M.H., Kim, J.S., and Sessler, J.L. (2015). Small molecule-based ratiometric fluorescence probes for cations, anions, and biomolecules. Chem. Soc. Rev. *44*, 4185–4191.

Lee, S.M., and An, W.S. (2016). New clinical criteria for septic shock: serum lactate level as new emerging vital sign. J. Thorac. Dis. *8*, 1388–1390.

Lelimousin, M., Noirclerc-Savoye, M., Lazareno-Saez, C., Paetzold, B., Le Vot, S., Chazal, R., Macheboeuf, P., Field, M.J., Bourgeois, D., and Royant, A. (2009). Intrinsic dynamics in ECFP and Cerulean control fluorescence quantum yield. Biochemistry *48*, 10038–10046.

Lerchundi, R., Fernandez-Moncada, I., Contreras-Baeza, Y., Sotelo-Hitschfeld, T., Machler, P., Wyss, M.T., Stobart, J., Baeza-Lehnert, F., Alegria, K., Weber, B., et al. (2015). NH4(+) triggers the release of astrocytic lactate via mitochondrial pyruvate shunting. Proc. Natl. Acad. Sci. U S A *112*, 11090–11095.

Liberti, M.V., and Locasale, J.W. (2016). The Warburg effect: how does it benefit cancer cells? Trends Biochem. Sci. *41*, 211–218.

Machler, P., Wyss, M.T., Elsayed, M., Stobart, J., Gutierrez, R., von Faber-Castell, A., Kaelin, V., Zuend, M., San Martin, A., Romero-Gomez, I., et al. (2016). In vivo evidence for a lactate gradient from astrocytes to neurons. Cell Metab. *23*, 94–102.

Magistretti, P.J., and Allaman, I. (2018). Lactate in the brain: from metabolic end-product to signalling molecule. Nat. Rev. Neurosci. *19*, 235–249.

Marzouk, S.A., Buck, R.P., Dunlap, L.A., Johnson, T.A., and Cascio, W.E. (2002). Measurement of extracellular pH, K(+), and lactate in ischemic heart. Anal. Biochem. *308*, 52–60.

Miller, D.M., Thomas, S.D., Islam, A., Muench, D., and Sedoris, K. (2012). c-Myc and cancer metabolism. Clin. Cancer Res. *18*, 5546–5553.

Ovens, M.J., Davies, A.J., Wilson, M.C., Murray, C.M., and Halestrap, A.P. (2010). AR-C155858 is a potent inhibitor of monocarboxylate transporters MCT1 and MCT2 that binds to an intracellular site involving transmembrane helices 7-10. Biochem. J. *425*, 523–530.

Paredes, R.M., Etzler, J.C., Watts, L.T., Zheng, W., and Lechleiter, J.D. (2008). Chemical calcium indicators. Methods *46*, 143–151.

Pedelacq, J.D., Cabantous, S., Tran, T., Terwilliger, T.C., and Waldo, G.S. (2006). Engineering and characterization of a superfolder green fluorescent protein. Nat. Biotechnol. *24*, 79–88.

Philp, A., Macdonald, A.L., and Watt, P.W. (2005). Lactate–a signal coordinating cell and systemic function. J. Exp. Biol. *208*, 4561–4575.

Proia, P., Di Liegro, C.M., Schiera, G., Fricano, A., and Di Liegro, I. (2016). Lactate as a metabolite and a regulator in the central nervous system. Int. J. Mol. Sci. *17*, 1450.

Roberts, T.M., Rudolf, F., Meyer, A., Pellaux, R., Whitehead, E., Panke, S., and Held, M. (2016). Identification and characterisation of a pH-stable GFP. Sci. Rep. *6*, 28166.

San Martin, A., Ceballo, S., Ruminot, I., Lerchundi, R., Frommer, W.B., and Barros, L.F. (2013). A genetically encoded FRET lactate sensor and its use to detect the Warburg effect in single cancer cells. PLoS One *8*, e57712.

Shaner, N.C., Steinbach, P.A., and Tsien, R.Y. (2005). A guide to choosing fluorescent proteins. Nat. Methods *2*, 905–909.

Sohal, D.S., Nghiem, M., Crackower, M.A., Witt, S.A., Kimball, T.R., Tymitz, K.M., Penninger, J.M., and Molkentin, J.D. (2001). Temporally regulated and tissue-specific gene manipulations in the adult and embryonic heart using a tamoxifen-inducible Cre protein. Circ. Res. *89*, 20–25.

Stepanenko, O.V., Stepanenko, O.V., Kuznetsova, I.M., Verkhusha, V.V., and Turoverov, K.K. (2014). Sensitivity of superfolder GFP to ionic agents. PLoS One *9*, e110750.

Sugiura, Y., Katsumata, Y., Sano, M., Honda, K., Kajimura, M., Fukuda, K., and Suematsu, M. (2016). Visualization of in vivo metabolic flows reveals accelerated utilization of glucose and lactate in penumbra of ischemic heart. Sci. Rep. *6*, 32361.

Takahashi, N., and Yamada, T. (1996). Catabolic pathway for aerobic degradation of lactate by Actinomyces naeslundii. Oral Microbiol. Immunol. *11*, 193–198.

Tasdogan, A., Faubert, B., Ramesh, V., Ubellacker, J.M., Shen, B., Solmonson, A., Murphy, M.M., Gu, Z., Gu, W., Martin, M., et al. (2019). Metabolic heterogeneity confers differences in melanoma metastatic potential. Nature *577*, 115–120.

Vardjan, N., Chowdhury, H.H., Horvat, A., Velebit, J., Malnar, M., Muhic, M., Kreft, M., Krivec, S.G., Bobnar, S.T., Mis, K., et al. (2018). Enhancement of astroglial aerobic glycolysis by extracellular lactate-mediated increase in cAMP. Front. Mol. Neurosci. *11*, 148.

Walenta, S., Wetterling, M., Lehrke, M., Schwickert, G., Sundfor, K., Rofstad, E.K., and Mueller-Klieser, W. (2000). High lactate levels predict likelihood of metastases, tumor recurrence, and restricted patient survival in human cervical cancers. Cancer Res. *60*, 916–921.

Yu, Q., Pourmandi, N., Xue, L., Gondrand, C., Fabritz, S., Bardy, D., Patiny, L., Katsyuba, E., Auwerx, J., and Johnsson, K. (2019). A biosensor for measuring NAD+ levels at the point of care. Nat. Metab. *1*, 1219–1225.

Zhang, C., Wei, Z.H., and Ye, B.C. (2013). Imaging and tracing of intracellular metabolites utilizing genetically encoded fluorescent biosensors. Biotechnol. J. *8*, 1280–1291.

Zhang, D., Tang, Z., Huang, H., Zhou, G., Cui, C., Weng, Y., Liu, W., Kim, S., Lee, S., Perez-Neut, M., et al. (2019). Metabolic regulation of gene expression by histone lactylation. Nature *574*, 575–580.

Zhao, Y., Araki, S., Wu, J., Teramoto, T., Chang, Y.F., Nakano, M., Abdelfattah, A.S., Fujiwara, M., Ishihara, T., Nagai, T., et al. (2011). An expanded palette of genetically encoded Ca(2)(+) indicators. Science *333*, 1888–1891.

Zhao, Y., Hu, Q., Cheng, F., Su, N., Wang, A., Zou, Y., Hu, H., Chen, X., Zhou, H.M., Huang, X., et al. (2015). SoNar, a highly responsive NAD+/NADH sensor, allows high-throughput metabolic screening of anti-tumor agents. Cell Metab. *21*, 777–789.

STAR★METHODS

KEY RESOURCES TABLE

REAGENT OR RESOURCE	SOURCE	IDENTIFIER
Antibodies		
β-tubulin	Sigma-Aldrich	#t5201 ; RRID:AB_609915
GFP	MBL	#598 ; RRID:AB_591819
anti-mouse secondary	Thermo-Fisher	#31430 ; RRID:AB_228307
anti-rabbit secondary	Thermo-Fisher	#31460 ; RRID:AB_228341
Bacterial and virus strains		
pCMV-dR7.2 dvpr	Addgene	#8455
pCMV-VSV-G	Addgene	#8454
LV-Cre-SD	Addgene	#12105 (no longer available)
pcDNA3.1	Life Technologies	cat no. V79020
pCold II	TaKaRa Bio	#3362
Ai38	Addgene	#34883
Rosetta DE3 Competent Cells	Novagen	#70956
XL10-Gold Cells	Agilent	#200315
Chemicals, buffer reagents, and recombinant proteins		
Tamoxifen	Sigma-Aldrich	T5648
Lenti-X concentrator	TaKaRa Bio	#631232
poly-ornithine	Sigma-Aldrich	#P0421
Lipofectamine 2000	Life Technologies	#11668027
Lipofectamine 3000	Life Technologies	#L3000008
OptiMEM	Thermo-Fisher	#31985070
Ni-sepharose Beads	GE Healthcare	#17-5318-01
IPTG	Sigma-Aldrich	I6758
Cell Lysis Buffer	Cell Signaling Technologies	#9803
Pierce ECL western blotting substrate	Thermo-Fisher	#32209
Superblock	Thermo-Fisher	#37515
Critical Commercial Assays		
Lactate Assay Kit	Sigma Aldrich	#MAK064
Experimental Models: Cell Lines		
Human: HEK 293T	ATCC	#CRL-3216
Human: NIH 3T3	ATCC	#CRL-1658
Experimental Models: Mouse Lines		
αMHC-MerCreMer	JAX	#005657
αMHC-Cre	JAX	#011038
Oligonucleotides		
Oligonucleotides designed in this study	Full sequence maps available upon request	N/A
Software and algorithms		
Vevo770	VisualSonics	N/A
iE33 Ultrasound	Philips	N/A
CueMol2	N/A	http://www.cuemol.org/
I-TASSER	Zhang Lab	https://zhanglab.ccmb.med.umich.edu/I-TASSER/
MetaFluor	Molecular Devices	Version 7.8.1.0
Prism v9.0	GraphPad	https://www.graphpad.com/

RESOURCE AVAILABILITY

Lead contact

Further information and requests for resources and reagents should be directed to and will be fulfilled by the Lead Contact Dr. Masayuki Yazawa (my2387@columbia.edu)

Materials availability

All materials and constructs used in this study are maintained by Dr. Yazawa's laboratory and are available upon request. In the future, the constructs and mouse line will be deposited and available to order through Addgene and JAX, respectively.

Data and code availability

- All data reported in this paper will be shared by the lead contact upon request.
- This paper does not report original code.
- Any additional information required to reanalyze the data reported in this paper is available from the lead contact upon request.

EXPERIMENTAL MODEL AND SUBJECT DETAILS

Mice

This study was carried out in strict accordance with the guidelines of the National Institutes of Health and the Institutional Animal Care and Use Committee at Columbia University, New York. The protocol was approved by the IACUC at Columbia University (protocol #AC-AAAU2453/AABK3550). All mice are housed under a 12 hour light/dark cycle and provided with food and water *ad libidum*. The synthesized C-GEM-IL 2.0/3.0 DNA fragment (Integrated DNA Technologies) was inserted into the Ai38 targeting construct (Addgene, #34883) utilizing the FseI restriction site (NEB, R0588S). The construct was then linearized using PvuI-HF digestion enzyme (NEB, R3150S). The linearized construct was electroporated into home-made mouse embryonic stem cells (C-S. L generated) using a standard protocol. The germ-line transmitted C-GEM-IL 2.0/3.0 mice were crossed with the αMHC-MerCreMer line (JAX #005657) or αMHC-Cre line (JAX #011038). In case of αMHC-MerCreMer use, the subsequent progeny was injected intraperitonially with 50mg/kg body weight of tamoxifen (Sigma-Aldrich, dissolved in sunflower oil, 1 dose/day, 3 days) to induce the cardiac specific expression of C-GEM-IL. Mouse primary adult ventricular myocytes were isolated from C-GEM-IL 2.0/3.0 mice using our established protocol. These cells were then calcium ion-adapted and imaged as described in the below perfusion section. Genomic DNA was extracted from the cardiac and tail samples from C-GEM-IL 2.0 and 3.0 positive mice using standard phenol/chloroform-ethanol precipitation method. The target sequence was then amplified evidencing the cardiac-specific Cre-lox recombination utilizing Ex Taq DNA polymerase (TaKaRa/Clontech, RR001B).

Cell culture

Human embryonic kidney (HEK) 293T cells (ATCC, #CRL-3216) and NIH 3T3 cells (ATCC, #CRL-1658) were cultured in Dulbecco's Modified Eagle Media (DMEM, Thermo-Fisher/Gibco #10313021) supplemented with GlutaMax-I and penicillin, streptomycin (PS) and 10% fetal bovine serum (FBS, not heat-inactivated, HyClone, #SH30071.03, Thermo-Fisher) under normoxia (20% O2, 5% CO2, at 37°C).

Human normal induced pluripotent stem cells (iPSCs) were cultured using a standard feeder-free protocol with Essential 8 medium and Geltrex (Thermo-Fisher/Gibco #A1517001) following the manufacturer's instructions. Human iPSC lines were differentiated using Neural Induction Media (NIM, Thermo-Fisher/Gibco #A1647801) to generate neural progenitor cells. The progenitors were cultured using NIM supplement, Neurobasal and advanced DMEM media (Thermo-Fisher/Gibco) following the NIM manufacturer's instruction.

METHOD DETAILS

Lactate biochemical assay

The lactate content of the cells and the media was measured using a lactate assay kit (Sigma-Aldrich/Millipore-Sigma, #MAK064) following the manufacturer's instructions. In brief, the cells were infected with the c-Myc virus for 24 hours. The cell media was then replaced by phenol red-free DMEM (Thermo-Fisher/Gibco, #31053028) supplemented with GlutaMax-I, PS and 10% FBS. Twenty-four hours later, the media and cells were harvested and filtered through a 10kDa filter (Amicon, UFC801024). The samples were then plated on a flat bottom 96-well plate (Falcon, #353072) and read using a plate reader Spectramax ID3 (Molecular Devices).

Plasmid DNA construction

Plasmid DNA constructs were generated using standard methods using restriction enzymes (New England BioLabs), DNA ligase (MightMix, TaKaRa) and polymerase chain reaction (PCR) with Phusion polymerase chain reaction (Thermo-Fisher, 2× master

mix) or gBlock DNA synthesis (IDT). The transient expression vector pcDNA3.1 (Life Technologies) was used for transient overexpression in mammalian cells, pCold II was for bacterial expression, and lentiviral vector LV-SD (Addgene, #12105, LV-Cre-SD, no longer available currently, Cre was removed by using EcoRI-XhoI sites) was for lentiviral expressions.

Lentiviral generation and infection of NPC and NIH 3T3 cells

Lentiviral production and infection were conducted using standard method. Briefly, HEK 293T cells were transfected with lentiviral human c-Myc vectors together with pCMV-dR7.2 dvpr and pCMV-VSV-G (Addgene #8455 & 8454). Lentivira c-Myc plasmid was generated using standard PCR and LV-SD with EcoRI and XhoI cloning sites. The lentivirus was then concentrated using a Lenti-X concentrator (TaKaRa/Clontech, #631232) following manufacturer's instructions to infect either neural progenitor cells or NIH 3T3 cells.

Plasmid DNA transfection

Plasmid transfection of HEK 293T and NIH 3T3 cells was conducted using standard lipofection method. Briefly, HEK 293T and NIH 3T3 cells were plated at $0.5x10^5$ cells/well in a 24-well plate format on poly-ornithine coated (Sigma-Aldrich/Millipore-Sigma, #P0421) glass cover slips (Warner instruments). HEK 293T cells were transfected with 0.9μg of DNA in 2μL of Lipofectamine 2000 (Invitrogen/Life Technologies #11668027) into 100μL of OptiMEM (Thermo-Fisher/Gibco #31985070) in 400μL: of DMEM 10% FBS (PS-free). NIH 3T3 cells were transfected with 0.5μg DNA, 1μL P3000 and 1.5μL Lipofectamine 3000 (Invitrogen/Thermo-Fisher #L3000008) into 50μL OptiMEM in 400μL of DMEM 10% FBS (PS-free).

Purification and characterization of recombinant protein

Recombinant forms of the indicator protein were purified through batch nickel purification taking advantage of the 6xHis tag (GE Healthcare #17-5318-01) in the pCold_2 vector. Briefly, Rosetta (DE3)pLysS Competent cells (Novagen #70956) were transfected with the pCold II vector with the respective inserts and grown at 37°C overnight. These primary cultures were then used for larger scale production at a 1:100 inoculation. The larger cultures were grown for 4-6 hours at 37°C (or until the O.D. was between 0.4-0.8). The cultures were then placed in ice for 1 hour, followed by addition of 0.5mM IPTG. These cold-shocked cultures were then placed in a 16°C shaker for 24 hours at 250 rpm. Samples were then spun down and resuspended in lysis buffer (20mM Na_3PO_4, 500mM NaCl, 20mM Imidazole, 1mM EDTA, 0.1% Triton X-100, 150mM sucrose) followed by sonication (Branson sonifier 450). The lysed samples were then then added to the beads, washed, and then eluted (elution buffer: 20mM Na_3PO_4, 500mM NaCl, 500mM Imidazole, 1mM EDTA, 150mM sucrose). The protein was then concentrated using centrifugal filters with a 10,000 Da (Amicon Ultra-15 UFC901024) cutoff and resuspended in cytoplasmic buffer (pH 7.0, 10mM NaCl, 130mM KCl, 1.25mM $MgSO_4$, 10mM HEPES). HEK 293T cells were transfected with C-GEM-IL 3.0 as described above. Forty-eight hours after transfection, the cells were lysed with cell lysis buffer (CST, #9803). The protein was then isolated with nickel beads similarly to that from bacteria. The purified recombinant protein (100 nM) was added to a flat black bottom 96-well plate (Costar 3916) in the respective solutions. The plates were then read in Spectramax ID3.

Fluorescent HPLC

Autosampler SIL-20ACHT was used to inject 100-μl protein samples into the Superose 6 10/30 gel filtration chromatography column connected to the Shimadzu HPLC. The samples were monitored using the RF-20A spectrofluorometric detector at the excitation wavelength of 435 nm and the emission wavelength of 485 nm.

Cellular perfusion experiments

Cultured cells were plated at $0.5 x10^5$ cells/well in a 24-well plate format on poly-ornithine coated glass cover slips. Cells were transfected as described above. For dual imaging experiments, cells were transfected with C-GEM-IL 3.0 and R-GECO1 simultaneously using the same transfection protocol. 24-48 hours following transfection cover slips were washed three times with normal Tyrode's solution three times (normal Tyrode's solution: 1.8mM $CaCl_2$, 1mM $MgCl_2$, 140mM NaCl, 5.4mM KCl, 10mM glucose, and 10mM HEPES (pH7.4 adjusted with NaOH at 25°C), After wash, the coverslips were picked and placed in the imaging chamber (Warner Instruments/Harvard Apparatus, RC-20H, #64-0223). Cells were imaged and fluorescence was traced throughout the perfusions using an inverted Nikon Eclipse Ti microscope with a Nikon 20x objective and MetaFluor Software Version 7.8.1.0 (Molecular Devices). Baseline fluorescence in Tyrode's solution was gathered for 300 seconds, followed by a 2 mL perfusion of the compound of interest dissolved in Tyrode's solution with recording for 300 seconds, followed by a 2 mL perfusion of Tyrode's solution as a wash. Changes in fluorescent data were quantified and analyzed relative to baseline in Excel.

Kinetic measurement

NIH 3T3 cells were plated on coverslips, transfected with C-GEM-IL 3.0, and placed in the imaging chamber set up as described above. Cells were again imaged using MetaFluor Software Version 7.8.1.0. A 150-second baseline was recorded in Tyrode's solution, followed by 2mL perfusions of increasing doses (1, 5, 10, 20, and 50mM) of sodium lactate dissolved in Tyrode's solution each recorded for 150 seconds. No pH changes were observed after adding 10-20mM sodium lactate into the Tyrode's solution. Changes in fluorescent data were quantified and analyzed relative to baseline in Excel.

Multi-filter fluorescent imaging

Cells were plated 1.5 x10^5 cells/dish in 35mm glass bottom poly-ornithine coated dishes. The cells were transfected as previously described. 24-48 hours post-transfection cells were washed three times with Tyrode's solution and then imaged using MetaMorph Imaging Software. A Sutter Lambda DG-4 Illumination System was used with standard BFP, CFP, GFP, and YFP filters (Chroma).

Hydrodynamic tail vein injection

5-6 week-old C-GEM-IL 3.0 positive mice were injected with PAC-Cre plasmid using TransIT ®-EE Delivery Solution (Mirus Bio LLC) respectively according to the manufacturer's protocol. The amount of injected plasmid DNA was 10μg per mouse. The volume of delivery solution was 0.1mL per mouse weight (g). After the hydrodynamic injection of DNA, the mice were allowed to recover for 48 hours. The mice were then sacrificed using standard procedure approved in our animal protocol and their livers were immediately harvested for protein expression characterization using Western blotting.

Echocardiographic measurements

Echocardiography was conducted using standard method. Briefly, C-GEM-IL mice were placed under light anesthesia (2% isoflurane) and imaged using Vevo 770 with a 40-MHz transducer (for C-GEM-IL 2.0) or iE33 with a 15-MHz linear transducer (for C-GEM-IL 3.0). M-mode images and two-dimensional parasternal short-axis images at the mid-papillary level were recorded in each mouse.

Homology modelling

The LldR lactate binding domain was determined using known templates in the SWISS-MODEL (Biozentrum) that produced a high identity with the transcriptional factor CGL2914 from Corynebacterium glutamicum (2DI3a). This was used to generate a homology model that was visualized using CueMol2.

Western blotting

Western blot experiments were conducted using standard method. In brief, cardiac/liver samples harvested from C-GEM-IL 2.0/3.0 positive and wild-type mice were homogenized and lysed in 10x cell lysis buffer (Cell Signaling Technology, #9803) with 1% protease inhibitor cocktail (Sigma-Aldrich/Millipore-Sigma). SDS-polyacrylamide gel electrophoresis was performed using Tris-Glycine-based gels (Bio-Rad) containing 10% Acrylamide-Bis (Fisher Scientific) which was then transferred to polyvinylidene difluoride (PVDF) membranes. Primary bodies to GFP (MBL#598, 1/4,000 dilution) and β-tubulin (Sigma-Aldrich, #t5201, 1/4000 dilution). Secondary antibody α-mouse (Invitrogen, #31430, 1/8,000 dilution) and α-rabbit (Thermo Scientific, #31430, 1/8,000 dilution). SuperBlock blocking buffer (PBS based, Thermo Scientific #37515) was used for blocking and antibody incubations of the PVDF membranes. Pierce ECL western blotting substrate (Thermo Scientific, #32209) was used for the chemiluminescent reaction.

QUANTIFICATION AND STATISTICAL ANALYSIS

Quantification of fluorescent intensity was done using MetaMorph software (Molecular Devices). Cellular regions were manually defined and quantified during a defined imaging study. Two-tailed Student's *t*-test was used when comparing two separate groups of observations. Welch's correction was used when the variance between the two groups was statistically different. Two-tailed paired Student's *t*-test was used when comparing data sets conducted on samples before and after treatment. One-way ANOVA with Bonferroni or Sidak's comparison corrections was used for comparison between multiple sets of observations. One-way ANOVA with Dunnet's correction was used for multiple comparisons against a specified data set. GraphPad Prism non-linear regression model of total site binding was used to generate dissociation constants. All error bars represented standard deviation. p values < 0.05 were considered significant. Unless otherwise stated, all experiments were conducted in at least three independent experiments.